NBSIR 75-664

Strength Degradation of Brittle Surfaces: Blunt Indenters

B. R. Lawn, S. M. Wiederhorn, and H. H. Johnson

Inorganic Materials Division
Institute for Materials Research
National Bureau of Standards
Washington, D. C. 20234

February 1975

Interim Report for Period July 1, 1974 through June 30, 1975

Prepared for
Department of the Navy
Office of Naval Research
Arlington, Virginia 22217

NBSIR 75–664

STRENGTH DEGRADATION OF BRITTLE SURFACES: BLUNT INDENTERS

B. R. Lawn, S. M. Wiederhorn, and H. H. Johnson

Inorganic Materials Division
Institute for Materials Research
National Bureau of Standards
Washington, D. C. 20234

February 1975

Interim Report for Period July 1, 1974 through June 30, 1975

Prepared for
Department of the Navy
Office of Naval Research
Arlington, Virginia 22217

U. S. DEPARTMENT OF COMMERCE, Frederick B. Dent, Secretary

NATIONAL BUREAU OF STANDARDS, Richard W. Roberts, Director

STRENGTH DEGRADATION OF BRITTLE SURFACES: BLUNT INDENTERS

B. R. Lawn*, S. M. Wiederhorn and H. H. Johnson

Institute for Materials Research
National Bureau of Standards
Washington, D. C. 20234 U.S.A.

*On study leave, from School of Physics, University of New South Wales, Kensington, N.S.W. 2033, Australia.

Abstract

Indentation fracture mechanics is used to develop a theoretical basis for predetermining the strength properties of brittle surfaces in prospective contact situations. Indenters are classified as "blunt" or "sharp", of which only the first is considered in the present work. The classical Hertzian cone crack conveniently models the fracture damage incurred by the surface in this class of indentation event. Significant degradation is predicted at a critical contact load; however, with increasing load beyond this critical level, further degradation occurs at a relatively slight rate. Bend tests on abraded glass slabs confirm the essential features of the theoretical predictions. The role of controlling variables in the degradation process, notably starting flaw size and indenter radius, is systematically investigated. An indication is also given as to optimisation of material parameters.

I. Introduction

The possible strength degradation of a brittle surface due to contact with a hard particle, especially in an impact situation, is an important consideration in ceramics engineering. A typical contact event may not in itself cause the failure of a structural component, but may nevertheless generate highly localized stresses of sufficient intensity to develop potentially dangerous cracks. With variables relating to particle geometry, loading conditions (e.g., load rate), mechanical properties of the materials, state of the brittle surface, etc. complicating the general issue, it is little wonder that a fundamental description of the problem has been slow in evolving.

However, the emergence within the past decade of the field of "indentation fracture mechanics," recently reviewed by Lawn and Wilshaw[1], establishes the necessary foundation for a theoretical analysis of contact-induced degradation. Evans[2] was the first to propose a theory along these lines, but his treatment addressed only one specific situation, that of impact loading with a hard spherical indenter, and did not explore the role of many important indentation variables. The present work was initiated in an effort to generalise the Evans analysis. The philosophy adopted here was that the strength properties of a material should be predictable from basic fracture parameters as determined from standard indentation tests.

To this end it is convenient, following the scheme of Ref. 1, to distinguish two extremes of indenter type: (i) "blunt indenters" (typified by a hard sphere), characterised by a perfectly elastic contact such that crack initiation is controlled by pre-existing flaws (usually at the specimen surface); (ii) "sharp indenters" (e.g., cone or pyramid), characterized by a partially plastic contact such that the starting flaws are produced by the actual indentation process itself. "Real contact situations" may then be viewed as lying somewhere between these two limits. We accordingly deal with only blunt indenters in this paper, and defer investigation of sharp indenters till a subsequent publication. For simplicity, crack growth is considered to occur under quasistatic conditions throughout, an assumption that should hold good for contact rates up to an appreciable fraction of sonic velocities.

II. The Spherical Indenter and Hertzian Cone Fracture

We consider the nature of the cracking that results from the contact between an elastic sphere (indenter) and an elastic-brittle surface (specimen). This is the most widely used test configuration of the classical Hertzian contact[1]. The elastic field, although complex, remains well-defined up to a critical load, at which point a cone-shaped crack suddenly develops in the specimen. Initiation of the cone crack invariably takes place at a pre-existing surface flaw located just outside the contact circle, where the tension is greatest. Fig. 1 indicates the basic test parameters.

The mechanics of cone extension through the inhomogeneous Hertzian field has been investigated in great detail, both theoretically and experimentally[3-10]. For the purpose of strength evaluation we need to know how the size of the cone crack varies with indenter load. It is convenient to consider the behavior prior and subsequent to critical loading in separate parts.

(1) Subcritical loading ($P \leq P_c$)

As the indenter load P steadily increases from its initial zero value the ultimate starting flaw will experience a tensile stress field of growing intensity. In the absence of kinetic effects in the crack growth the condition for sudden development of the surface flaw into a propagating cone may be readily formulated in terms of the fundamental, equilibrium energy-balance criterion of Griffith[11]: essentially, the cone develops when the crack-extension force associated with the applied loading exceeds the resistance term associated with the creation of new surface area. Because of the strong inhomogeneity of the Hertzian field, it is no simple matter to derive a single, exact analytical relation for the critical load as a function of starting flaw size. However, one can obtain working expressions for the limiting cases of "small" and "large" flaws[1, 3]:

(a) Small flaws. For surface flaws of effective initial length c_f^o very small in comparison with the scale of the elastic field (typically, $c_f^o << 0.01\ a$, where a is the contact radius[3]) the gradient of stress along the crack trajectory may be considered to be negligibly small. In other words, the flaw will tend to respond as if it were located in a field of uniform tension. Thus, when the tensile strength of the material is exceeded at the site of the flaw unstable crack propagation ensues,

and the cone accordingly develops spontaneously until a position of stability is once more attained remote from the contact area. On the assumption that initiation is favored at the surface location of maximum tensile stress, i.e, at the contact circle, the Hertzian equations predict[1, 3, 5, 6]

$$P_c = \Gamma^{3/2} k^2 r^2 / \chi(\nu) E^{1/2} c_f^{o\ 3/2} \qquad (c_f^o << 0.01a); \qquad (1)$$

here Γ is the fracture surface energy, $k = (9/16)\left[(1-\nu^2)+(1-\nu'^2)E/E'\right]$ is a dimensionless constant with ν Poisson's ratio and E Young's modulus (the primes refering to the indenter material), r is the sphere radius and $\chi(\nu) = \{(3/4)\left[3(1-\nu^2)(1-2\nu)^2/32\pi\right]^3\}^{1/2}$ is another dimensionless constant. We note in particular the dependence of the critical load on flaw size and ball radius.

(b) Large flaws. For flaws sufficiently large that the (negative) gradient of tensile stress along their length becomes appreciable (typically, $c_f^o \gtrsim 0.01a$) the approximation of a uniform field is no longer valid. Instead, there is a tendency to limited initial growth of the flaw as a stable surface ring just prior to cone formation[3, 7]. That is, the crack must first surmount an energy barrier before it can become unstable, and the condition for this to occur may again be evaluated from the Hertzian equations[1, 3-6]

$$P_c = 2\Gamma kr/\phi^*(\nu) = Ar \qquad (c_f^o \gtrsim 0.01a), \qquad (2)$$

where $\phi^*(\nu)$ is another dimensionless constant whose value can be estimated (but only to within an order of magnitude) by numerical analysis, and A is a material constant known as Auerbach's constant after the discover of the empirical "law" $P_c \propto r$ in 1891[12]. The dependence of the critical load on ball size is, therefore, less marked in the large-flaw region. The same is true of the dependence

on flaw size; indeed, $\underline{c}_f^o$ has no direct influence on $\underline{P}_c$ at all in Eqn. (2).

The predictions of Eqns. (1) and (2) are represented in Fig. 2. In reality, the transition between the two regions of behavior is not as sharply defines as the analysis above would suggest. This is indicated in Fig. 2 by means of an experimental curve, evaluated from some data on glass[9]. (These data, and indeed the data described in the present work, will be seen to fall more within the realm of Eqn. (2) than of Eqn. (1).) Accordingly, the theory will generally underestimate the true value of $\underline{P}_c$, so that our ultimate estimates of strength will be on the conservative side.

Throughout the subcritical stage, $\underline{P}<\underline{P}_c$, therefore, we may expect little or no degradation of the brittle surface. It is true that limited stable extension of surface flaws might occur just prior to critical loading, but any such extension is predicted to be imperceptibly small[3], and will tend to be obscured in the general variation of flaw sizes sampled in the typical strength test.

(2) Supercritical loading ($\underline{P}>\underline{P}_c$)

Once the critical load is exceeded the crack grows substantially (typically, $\underline{R}>2\underline{a}$, Fig. 1). For the limiting case of a true cone (i.e, $\underline{R}_o \to 0$) the mechanics of fracture become independent of affairs within the contact zone (i.e., of $\underline{r}$ and $\underline{c}_f^o$), as seen in the simple equilibrium relation obtained by Roesler[10],

$$P^2/R^3 = 2\Gamma E/\kappa_R(\nu) \qquad (R>>R_o) \qquad (3)$$

where $\kappa_R(\nu)$ is a dimensionless term which can be computed (to within a factor of about two) by numerical methods[1]. Evans[2] and others have analyzed more general cone configurations, but the expressions derived tend to be unwieldy. Moreover, the Roesler formula underestimates the indenter load necessary to maintain the cone at a

prescribed depth, so that our strength estimates will once again be conservative ones.

III. Strength Degradation Tests

The strength of a brittle solid is defined in terms of the applied stress required to break a test piece in uniform tension. From the Griffith energy-balance condition one obtains the standard expression

$$\sigma = \left[2\Gamma E/\pi(1-\nu^2)c_f\right]^{1/2}, \qquad (4)$$

where σ is the applied stress and c_f is the effective length of the dominant flaw. This an equilibrium expression involving material properties and surface state. The strength will accordingly be reflected to some extent in the microstructural influence on Γ (possibly also on E), but to a much greater degree in the influence of a wide range of past mechanical, thermal and chemical events on c_f. Most ceramic surfaces contain a diversity of surface flaws, up to 10μm deep in even carefully handled test pieces; of these it is the weakest which determines the strength.

Since the prime concern in the present work was a systematic investigation of the factors affecting the mechanics of degradation, all strength tests were conducted under controlled surface conditions after the manner of Mould and Southwick[13, 14]. Soda-lime glass was selected as a test material, mainly because of the availability of reliable data on its fracture properties[1, 15] (but also for reasons of economy, mechanical isotropy and absence of microstructural complications). The test pieces were laths 250x37.5x5.65 mm, suitable for fracture in four-point bending with major span 204mm and minor

span 37.5 mm. A center spot approximately 15mm in diameter was grit blasted with a given grade of silicon carbide abrasive on each tension face prior to testing, thereby introducing a more or less uniform density of starting flaws for the ensuing fracture. By covering the abraded spot with a drop of paraffin oil immediately after the blast treatment any effects of moisture-assisted slow crack growth during subsequent testing could be largely eliminated. The bulk of the specimens were indented within the abrasion area with a tungsten carbide sphere of prescribed radius, at a preselected load, before rupture in bending. The delay between grit blasting and ultimate rupture never exceeded four hours.

(1) Strength of abraded test pieces

Strength tests were conducted on some non-indented specimens to establish the reproducibility of the grit-blast treatment, and to determine the effective length of the flaws resulting from this treatment. In most cases the fracture could be unambiguously traced to an origin within the central abrasion spot, but a few isolated examples of premature edge failures were encountered; these latter were rejected from the data accumulation. Table I summarizes the results. The scatter in measured strengths for each grit size, viz. less than ten percent, will be seen to be small compared to the magnitude of the degradation effect to be investigated in the following subsection. The effective lengths of the abrasion flaws, $\underline{c}_f = \underline{c}_f^o$ (grit size), then follow from Eqn. (4), using $\underline{E} = 7.0 \times 10^{10}$ Nm^{-2}, $\underline{\nu} = 0.25$ and $\underline{\Gamma} = 3.9$ Jm^{-2} for glass[15]. Microscopic examination of the grit-blasted areas showed individual microcrack damage centers of dimensions consistent with those listed in Table I.[14]

(2) Strength of indented test pieces

The effect of indentation load on strength was systematically investigated in a series of runs on glass specimens under conditions of given pre-abrasion treatment and sphere radius. In all such runs the strength remained essentially unaffected up to a critical indentation load, beyond which it showed a steady decline. This picture is consistent with the theoretical description outlined earlier: for $\underline{P} \leq \underline{P}_c$ (Section II (1)), we would predict the effective length of the dominant flaw to hold constant at the characteristic size of the abrasion damage, i.e., $\underline{c}_f = \underline{c}_f^o$; similarly, for $\underline{P} > \underline{P}_c$ (Section II (2)), we would predict the effective flaw length to be governed by the geometry of the newly propagating cone crack, i.e, $\underline{c}_f = \underline{c}_f(\underline{R}, \underline{\alpha})$ (Fig. 1). A more detailed analysis of the effectiveness of the conical crack as an initiating center for catastrophic failure in a tensile field can be given in terms of standard fracture mechanics formulae (Appendix); we obtain, at $\underline{R} >> \underline{R}_o$, $\underline{c}_f = \underline{R}\ \underline{\Omega}(\underline{\alpha})$, where $\underline{\Omega}(\underline{\alpha})$ is an angular-dependent dimensionless function (evaluated in the Appendix). Taken in conjunction with Eqn. (3), this term then gives the effective flaw size as a function of identation load. The strength equation (4) accordingly becomes

$$\sigma = [2\Gamma E/\pi(1-\nu^2)\ c_f^o]^{1/2}, \qquad (P<P_c), \qquad (5a)$$

$$\sigma = \{(2\Gamma E)^{2/3}/\Omega(\alpha)^{1/2}\ [\pi(1-\nu^2)]^{1/2}\ K_R(\nu)^{1/6}\}P^{-1/3} \quad (P>P_c). \qquad (5b)$$

These relations, together with Eqns. (1) and (2), provide, in principle, the basis for predetermining the degradation behavior without resort

to extensive (and, for all but the most common ceramic materials, expensive) failure testing under simulated service conditions.

Apart from the quantities $\underline{E}$, $\underline{\nu}$ and $\underline{\Gamma}$ already specified, the information necessary for a complete evaluation of our expressions may be obtained using straightforward indentation testing methods[1]. Typical values for a tungsten carbide sphere on a soda-lime glass specimen are as follows: $\underline{k} = 0.55$ and $\underline{\chi} = 5.1 \times 10^{-4}$ (calculable directly from the elastic constants); $\underline{\alpha} = 22\pm1°$ (direct observation of cone angle[3]), giving $\underline{\Omega} = 0.25\pm0.02$ (Appendix); $\underline{\phi} = (1.7\pm0.2) \times 10^{-5}$ (from tests on No. 320 grit-blasted glass in oil, $\underline{A} = (390\pm35)$N/1.58mm, Eqn.(2)); and $\underline{\kappa}_R = (1.3\pm0.2) \times 10^{-3}$ (vacuum observations of fully developed cone crack[1]).* This leaves the abrasion flaw size $\underline{c}_f^o$ and sphere radius $\underline{r}$ as convenient test variables for investigation here:

(a) Effect of flaw size. The first set of indentation/strength tests was conducted to investigate the role of initial flaw size on the ultimate degradation. The experimental results (data points) are compared with the theoretical predictions of Eqn. (5) (full lines) in Fig. 3, for a sphere of radius 1.58mm. We may note the following points of interest concerning the correlation in the different regions of behavior: (i) At $\underline{P}<\underline{P}_c$, there is no detectable degradation, as predicted (other than the usual deterioration associated with

*As indicated in Section II it is possible to compute values of these dimensionless constants directly from a knowledge of the Hertzian elastic stress field using basic fracture mechanics. However, the degree of uncertainty in absolute values thus computed is currently such that direct experimental calibration affords by far the more reliable data[1].

increasing severity of the preabrasion treatment). (ii) At $P=P_c$, the strength cut-off point is observed to be reasonably independent of the abrasion flaw size[5] (although small, systematic deviations from constancy in P_c are apparent at the larger flaw sizes). This is consistent with behavior in the Auerbach domain (Table II). (iii) At $P>P_c$, the strength data asymptotically approaches the (flaw-size independent) limiting curve for true cones. The degradation is seen to be remarkably slight considering the intensity of loading supported by the glass during indentation. However, above loads of 3kN the experiment tended to end abruptly due to sudden failure of either indenter or specimen.

(b) Effect of sphere radius. A second set of tests was run to investigate the influence of indenter size. Data and theory are represented in Fig. 4, for an abrasion flaw size 10μm. Considering the different regions of behavior as before, we have: (i) At $P<P_c$, negligible degradation. (ii) At $P=P_c$, the fall-off point scales with sphere radius, once more in accord with Auerbach behavior (Table III). (iii) At $P>P_c$, an asymptotic approach to the limiting curve is again observed (this occurring more rapidly with diminishing indenter scale, with the smallest spheres producing a slight tendency to overshoot below the calculated curve). Again, the limits to data accumulation were determined by an abrupt failure during indentation.

IV. Discussion

Within the limits of the assumptions embodied in the Hertzian fracture model, our analysis establishes a conservative basis for

predetermining the strength properties of brittle ceramics in contact situations involving blunt indenters. In addition, it provides an indication as to which materials might be expected to suffer the least degradation. Thus, according to Eqns. (1) and (2), the onset of strength loss many be suppressed to a certain extent by choosing materials with large Γ and ν (larger ν leading to smaller χ in Eqn. (1), ϕ in Eqn. (2)[9]). Again, according to Eqn. (5), the strength loss once degradation does occur may be minimized at large Γ (Γ being influenced by microstructure, e.g., grain size) and ν (larger ν diminishing κ in Equation (5)), and also large E. That is, the material should be tough and stiff, with a large Poisson's ratio to restrain the development of a high level of tensile stress in the indentation field.*

However, for a given indenter the most practical means of controlling the prospective degradation is via the state of the brittle surface. As seen in Fig. 3, the size of the starting flaw, once above the 10μm level typical of ceramic surfaces, does not enter as a sensitive factor in the reckoning of strength degradation. Indeed, we may note that, if anything, the critical load for the onset of significant degradation is greater for the more severely abraded surfaces. This is in agreement with previous observations of the function $P_c(c_f^o)$, as indicated by the experimental curve in Fig. 2; indeed, it seems that a ten-fold increase in flaw size can lead to a two-fold increase in critical load in certain

*At the limiting value ν=0.5, the tensile component in the general indentation field disappears altogether[16].

favorable cases". While such behavior may be contrary to intuitive expectation, a logical explanation is to be found in the very factor responsible for the Auerbach relation Eqn. (2), namely, the inhomogenious nature of the Hertzian field. Basically, for very large flaws (typically, $c_f^o \gtrsim 0.1a$) the stress gradients in the indentation field can reach the point where the component of normal stress along the flaw length actually changes from tensile at the surface to compressive below the surface[9]; such flaws will accordingly propagate less easily than smaller flaws contained entirely within the region of complete tension near the indented surface. This result is interesting in that it suggests deliberate, severe pre-abrasion treatment as a potential means of inhibiting the onset of degradation. (At the same time, however, such treatment would, of course, weaken the material in flexure, etc.)

The present analysis, although quasistatic, may be usefully extrapolated to certain time-dependent contact situations. Impact-induced damage is an important practical case in point. Here, the quasistatic approximation should hold provided the rate of contact does not approach the velocity of elastic waves. The impact conditions under which such extrapolation may be made are currently under investigation. The advantages of using characteristic indentation fracture parameters obtained in simple, hardness testing routines to predict more complex phenomena involving in-service damage events are self-evident. Once the velocity of projectile impingement approaches sonic values, the problem becomes a dynamic one, and our analysis becomes invalid.

There are other time-dependent features in the cone-crack growth which cause further complication in the general description.

In particular, we have specifically avoided consideration of complex, non-equilibrium crack configurations. Kinetic crack extension can occur in a wide range of ceramic materials, notably as a result of crack-tip interactions with hostile environments. This is especially true of silicate glasses, where ambient moisture causes subcritical cracks to propagate at substantial velocities (typically, up to $1 mm\ s^{-1}$)[17]. Our procedure of administering a thin film of oil to the abraded glass surfaces to restrict access of moisture to the cracks therefore limits the range of applicability of the calculations in their present state. Nevertheless, some of the most important practical degradation situations would appear to be sufficiently well simulated in the present experimental arrangement: the case of impact already mentioned, where the duration of contact is too brief for environmental effects to manifest themselves, and operations under inert or vacuum condition (e.g., spacecraft), are just two examples.

In relating to practical problems one must also give consideration to the history of a ceramic component subsequent to any contact event. Indentation-induced cracks are susceptible to mechanical or thermal shock; stepwise repropagations can occur, thereby enlarging apparently innocuous cracks to potentially dangerous dimensions.[18] On the other hand, some cracks may actually close up and heal, either spontaneously if sufficiently fast running that contaminants do not penetrate along the interface, or via mass transport at elevated temperatures[18, 19].

One further point needs to be brought out here. As mentioned in Section III (2), the glass test pieces were prone to sudden failure at high indentation loads (that is, if the spherical indenter did not itself fail first). An examination of indented surfaces invariably revealed a pattern of radial cracks extending outward from the contact center just prior to the failure event. This was especially noticeable for the smaller indenters; indeed, in the case of the sphere of radius 0.40mm in Fig. 4 radial cracking was evident at loads not much in excess of the critical value for cone formation, and appeared to be associated with the slight tendency for the data points to overshoot the predicted degradation curve. Such radial crack patterns are more typical of sharp indenters. Evidently, at suitably high loads small spheres are capable of producing irreversible flow in the material, and thus of penetrating the surface[1]; this is aided by the fact that the expanding contact area tends to encompass the surface trace of the cone crack at higher loads, and thereby to suppress further cone extension. Since this alternative crack system is potentially more degrading than the cone crack system it demands closer examination. This provides the topic for the second paper in this study.

Finally, brief comment may be made on a certain similarity between the strength degradation curves described here for indentation damage and those described by Hasselman[20] for thermal shock. In both cases there exists a range of "loading" (i.e., a load-range limit, ΔP, or temperature range, ΔT) over which little if any degradation is apparent.

At a critical load, both descriptions imply an abrupt drop-off in strength, followed by a more gradual decrease with further load increase. A common feature of the indentation and thermal shock situations at subcritical loading is the availability of an amount of strain energy insufficient for unstable crack propagation. The condition for ultimate crack arrest once a supercritical condition has been exceeded is, however, somewhat different for the two cases, being due to a rapid (approximately inverse-square) fall-off in the stress field about the contact point in the indentation operation, and to the "fixed grips" nature of the loading in thermal shock. Further differences also arise from a somewhat different role of initiating surface flaws in the two cases.

Acknowledgements

The authors are indebted to A. G. Evans for motivating discussions in the early stages of this work, and to E. R. Fuller for assistance throughout. The sponsorship by the Office of Naval Research under Contract No. NR-032-535 is also acknowledged.

Appendix

The mode of failure of a cone-shaped crack in a uniform tensile stress field has been given only a cursory consideration.[2] Full-scale fracture expected to initiate from one of two diametrically opposite positions on the base rim of the cone coincident with the symmetry plane containing the axes of intial contact loading and subsequent flexural tension. We may obtain an approximate solution for this configuration by disregarding the crack curvature on either side of any such favored position, considering instead the representative case of a plane crack of half-length C, width infinity (parallel to the crack front), inclination α to the tensile axis. The scheme is shown in Fig. A1.

We are now in a position to apply standard fracture mechanics procedures to the problem[21]. The stress-intensity factors for an inclined plane crack in uniform tension are

$$\left.\begin{aligned} K_I &= \sigma(\pi C)^{1/2} \sin^2 \alpha \\ K_{II} &= \sigma(\pi C)^{1/2} \sin\alpha \cos\alpha \end{aligned}\right\} \qquad \text{(A1)}$$

where the subscripts denote I, "opening", and II, "sliding", modes of fracture. (Actually, since our representative configuration strictly involves an edge crack, an additional multiplying factor ≈ 1.12 should appear on the right side of the expressions in Eqn. (A1)[20]. However, this is nullified to some extent by a further factor, smaller than unity, arising from the curvature in the cone crack situation.) The present problem is complicated by the fact that the crack will not, in general, extend in its own plane; rather, it will tend to extend at some energetically favorable tilt angle θ,

as indicated in Fig. A1. This complication can be handled by regarding the critical incremental extension as a reinitiation process in the near field of the original crack[22]. We note that the incremental crack experiences both opening and sliding types of local stress:

$$\left.\begin{aligned} \sigma_{\theta\theta} &= [K_I/(2\pi r)^{1/2}]f^I_{\theta\theta} + [K_{II}/(2\pi r)^{1/2}]f^{II}_{\theta\theta} = K_I'/(2\pi r)^{1/2} \\ \sigma_{r\theta} &= [K_I/(2\pi r)^{1/2}]f^I_{r\theta} + [K_{II}/(2\pi r)^{1/2}]f^{II}_{r\theta} = K_{II}'/(2\pi r)^{1/2} \end{aligned}\right\} \quad (A2)$$

where the f terms are the angular-dependent components of the standard crack-tip stress formulae[21,22],

$$\left.\begin{aligned} f^I_{\theta\theta} &= \cos^3(\theta/2) \\ f^I_{r\theta} &= \sin(\theta/2)\cos^2(\theta/2) \end{aligned}\right\} \quad \text{(mode I)} \quad (A3)$$

$$\left.\begin{aligned} f^{II}_{\theta\theta} &= -3\sin(\theta/2)\cos^2(\theta/2) \\ f^{II}_{r\theta} &= \cos(\theta/2)[1-3\sin^2(\theta/2)] \end{aligned}\right\}, \quad \text{(mode II)} \quad (A4)$$

and the "transformed stress-intensity factors" K_I' and K_{II}' define the field for the modified crack. From (A2) and (A1) we have

$$\left.\begin{aligned} K_I'(\theta,\alpha) &= \sigma(\pi C)^{1/2}[f^I_{\theta\theta}\sin^2\alpha + f^{II}_{\theta\theta}\sin\alpha\cos\alpha] \\ K_{II}'(\theta,\alpha) &= \sigma(\pi C)^{1/2}[f^I_{r\theta}\sin^2\alpha + f^{II}_{r\theta}\sin\alpha\cos\alpha] \end{aligned}\right\}. \quad (A5)$$

Now to determine the energetically most favorable path from the original crack tip we compute the mechanical-energy-release rate G per unit width of crack front as a function of angular variation,

$$G(\theta, \alpha) = [(1-\nu^2)/E][K_I'^2(\theta, \alpha) + K_{II}'^2(\theta, \alpha)]. \quad (A6)$$

For a given inclination angle α, we may assume that for isotropic solids the crack will extend at that angle θ^* which gives a maximum $G^*(\alpha)$ in the energy release, i.e.

$$\partial G/\partial \theta = 0. \qquad \text{(A7)}$$

This equation, in conjunction with Eqns. (A5), (A4) and (A3) reduces Eqn. (A6) to the form

$$G^*(\alpha) = [\pi(1-\nu^2)\sigma^2 C/E]\omega(\alpha), \qquad \text{(A8)}$$

where $\omega(\alpha)$ is a dimensionless constant whose value attains a limiting value unity for normal cracks.

Equation (A8) then leads directly to the strength equation (4) of the text if the Griffith energy-balance condition

$$G^* = 2\Gamma \qquad \text{(A9)}$$

is satisfied, and if we write

$$c_f = C\ \omega(\alpha) \qquad \text{(A10)}$$

as the effective length of the flaw. In the limit of well-developed cones ($R \gg R_o$, Fig. 1) we have

$$C = R/\cos\alpha. \qquad \text{(A11)}$$

Thus, from (A10) and (A11),

$$c_f/R = \omega(\alpha)/\cos\alpha \equiv \Omega(\alpha). \qquad \text{(A12)}$$

The quantity $\Omega(\alpha)$ therefore defines our required angular term in Eqn. (5) of the text. Both Ω and θ^*, evaluated numerically, are plotted in Fig. A2. For the special case of α=22° (glass), we compute Ω=0.25, θ^*=-63°. An independent, empirical evaluation from strength data by Evans[2] yields Ω=0.20. Since Ω ultimately appears in the degradation formula Eqn. (5b) under a square root, uncertainties in the above analysis will not be of major significance .

References

1. B. R. Lawn and T. R. Wilshaw, "Indentation Fracture: Principles Applications," J. Mater. Sci., in press

2. A. G. Evans, "Strength Degradation by Projectile Impacts," J. Am. Ceram Soc., 56 [8] 405-409 (1973).

3. F. C. Frank and B. R. Lawn, "On the Theory of Hertzian Fracture," Proc. Roy. Soc. Lond., A299 [1458] 291-306 (1967).

4. B. R. Lawn, "Hertzian Fracture in Single Crystals with the Diamond Structure," J. Appl. Phys., 39 [10] 4828-4836 (1968).

5. F. B. Langitan and B. R. Lawn, "Hertzian Fracture Experiments on Abraded Glass Surfaces as Definitive Evidence for an Energy Balance Explanation of Auerbach's Law," J. Appl. Phys., 40 [10] 4009-4017 (1969).

6. T. R. Wilshaw, "The Hertzian Fracture Test," J. Phys. D.: Appl. Phys., 4 [10] 1567-1581 (1971).

7. A. G. Mikosza and B. R. Lawn, "Section-and-Etch Study of Hertzian Fracture Mechanics," J. Appl. Phys., 42 [13] 5540-5545 (1971).

8. J. S. Nadeau, "Hertzian Fracture of Vitreous Carbon," J. Am. Ceram. Soc., 56 [9] 467-472 (1973).

9. B. R. Lawn, T. R. Wilshaw and N. E. W. Hartley, "A Computer Simulation Study of Hertzian Cone Crack Growth," Intl. J. Fract. Mech., 10 [1] 1-16 (1974).

10. F. C. Roesler, "Brittle Fractures Near Equilibrium," Proc. Phys. Soc., B69 [10] 981-992 (1956).

11. A. A. Griffith, "The Phenomena of Rupture and Flow in Solids," Phil. Trans. Roy. Soc. Lond., A221, 163-198 (1920).

12. F. Auerbach, "Measurement of Hardness," Ann. Phys. Chem., 43, 61 (1891).

13. R. E. Mould and R. D. Southwick, "Strength and Static Fatigue of Abraded Glass Under Controlled Ambient Conditions: I. General Concepts and Apparatus," J. Am. Ceram. Soc., 42 [11] 542-547 (1959).

14. R. E. Mould and R. D. Southwick, "Strength and Static Fatigue of Abraded Glass Under Controlled Ambient Conditions: II. Effect of Various Abrasions and the Universal Fatigue Curve," J. Am. Ceram. Soc., 42 [11] 582-592 (1959).

15. S. M. Wiederhorn, "Fracture Surface Energy of Glass," J. Am. Ceram. Soc., 52 [2] 99-105 (1969).

16. B. R. Lawn and M. V. Swain, "Microfracture Beneath Point Indentations in Brittle Solids," J. Mater. Sci., in press.

17. S. M. Wiederhorn, "Influence of Water Vapor on Crack Propagation in Soda-lime Glass," J. Am. Ceram. Soc., 50 [8] 407-414 (1967).

18. S. M. Wiederhorn, B. J. Hockey and D. E. Roberts, "Effect of Temperature on the Fracture of Sapphire," Phil. Mag., 28 [4] 783-795 (1973).

19. B. J. Hockey and B. R. Lawn, "Electron Microscopic Observations of Microcracking About Indentations in Aluminum Oxide and Silicon Carbide," J. Mater. Sci., in press.

20. D. P. H. Hasselman, "Unified Theory of Thermal Shock Fracture Initiation and Crack Propagation in Brittle Ceramics," J. Am. Ceram. Soc., 52 [11] 600-604 (1969).

21. P. C. Paris and G. C. Sih, "Stress Analysis of Cracks," Am. Soc. Test. Mater., Spec. Tech. Publ. 381, 30-83 (1965).

22. B. R. Lawn and T. R. Wilshaw, Fracture of Brittle Solids, Cambridge University Press, Cambridge, 1975, Ch. 3.

Table I. Strength and effective flaw size (mean value ± standard deviations for at least ten tests per run) of glass test pieces preabraded in SiC grit blast at air pressure 0.275 MNm^{-2}. Bend tests in oil environment at Instron crosshead speed 50mm min^{-1}.

Grade SiC grit	Strength, $\underline{\sigma}/MNm^{-2}$	Flaw size, $\underline{c}_f^o/\mu m$
100	79±7	23±5
150	86±4	19±3
200	94±7	16±3
240	107±9	12±2
320	123±5	10±1

Table II. Critical leads to cone fracture, computed from Eqns. (1) and (2) for soda-lime glass for given indenter $\underline{r}$ =1.58mm, as function of flaw size. Note that $\underline{P}_c$ (Eqn. (2))>$\underline{P}_c$(Eqn. (1)) for all $\underline{c}_f^o$; i.e., data lie in "Auerbach region" (see Fig. 2).

Flaw size, $\underline{c}_f^o$ /μm	23	19	16	12	10
$\underline{P}_c$/N (Eqn. (1))	0.4	0.5	0.7	1.0	1.4
$\underline{P}_c$/N (Eqn. (2))	390	390	390	390	390

Table III. Critical loads to cone fracture, computed from Eqns. (1) and (2) for soda-lime glass for given flaw size c_f^o = 10μm, as function of indenter radius. Note that P_c > (Eqn. (2)) > P_c (Eqn. (1)) for all r, i.e., data lie in "Auerbach region".

Indenter radius, r/mm	6.34	3.17	1.58	0.79	0.40
P_c/N (Eqn. (1))	22	5.5	1.4	0.3	0.1
P_c/N (Eqn. (2))	1560	780	390	195	98.5

Figure Captions

1. Hertzian cone crack parameters.

2. Critical load to cone fracture as function of starting flaw size. Limiting cases of Eqns. (1) and (2) shown as full, straight lines. (Note, controlling equation is determined by which predicts the larger value of $\underline{P}_c$.) Real behavior shown as curve. (Note "tail" at large $\underline{c}_f^o$ in real curve.)

3. Strength degradation as function of indentation load, for given WC sphere, $\underline{r}$ = 1.58mm, on soda-lime glass surfaces containing different abrasion flaw sizes (indicated). Oil environment. Crosshead speed for indentation tests 0.5mm min^{-1}, for bend tests 50mm min^{-1}.

4. Strength degradation as function of indentation load, for soda-lime glass surfaces containing given abrasion flaws $\underline{c}_f^o$ = 10μm, using WC spheres of different radii (indicated). Oil environment. Crosshead speed for indentation tests 0.5mm min^{-1}, for bend tests 50mm min^{-1}.

A1. Plane-crack representation of Hertzian cone configuration (side view). One seeks the crack increment at ($\underline{r}$, $\underset{\sim}{\theta}$), with respect to origin at tip of representative crack, which optimizes energy release conditions.

A2. Angular terms for cone-crack extension in tensile field.

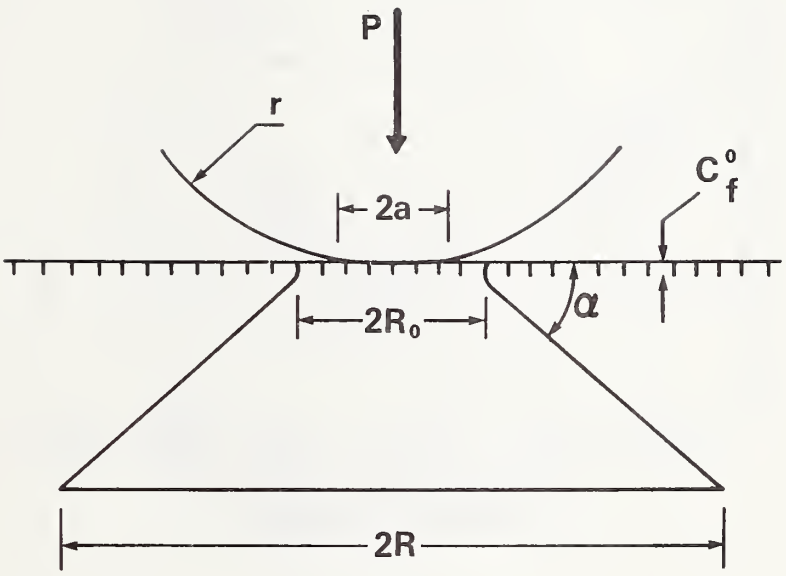

1. Hertzian cone crack parameters.

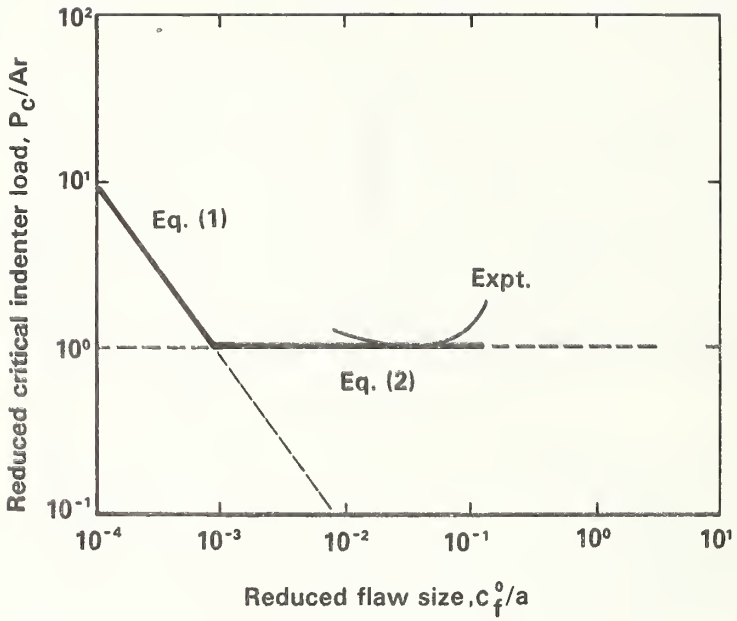

2. Critical load to cone fracture as function of starting flaw size. Limiting cases of Eqns. (1) and (2) shown as full, straight lines. (Note, controlling equation is determined by which predicts the larger value of P_c.) Real behavior shown as curve. (Note "tail" at large c_f^o in real curve.)

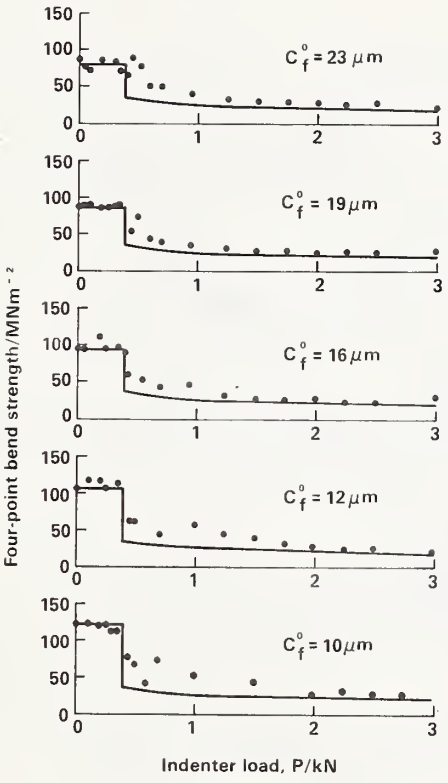

3. Strength degradation as function of indentation load, for given WC sphere, r = 1.58mm, on soda-lime glass surfaces containing different abrasion flaw sizes (indicated). Oil environment. Crosshead speed for indentation tests 0.5mm min^{-1}, for bend tests .50mm min^{-1}.

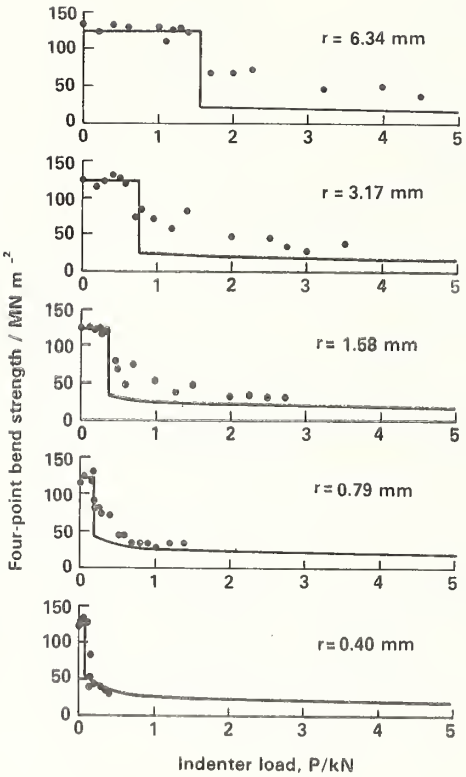

4. Strength degradation as function of indentation load, for soda-lime glass surfaces containing given abrasion flaws c_f^o = 10μm, using WC spheres of different radii (indicated). Oil environment. Crosshead speed for indentation tests 0.5mm min^{-1}, for bend tests 50mm min^{-1}.

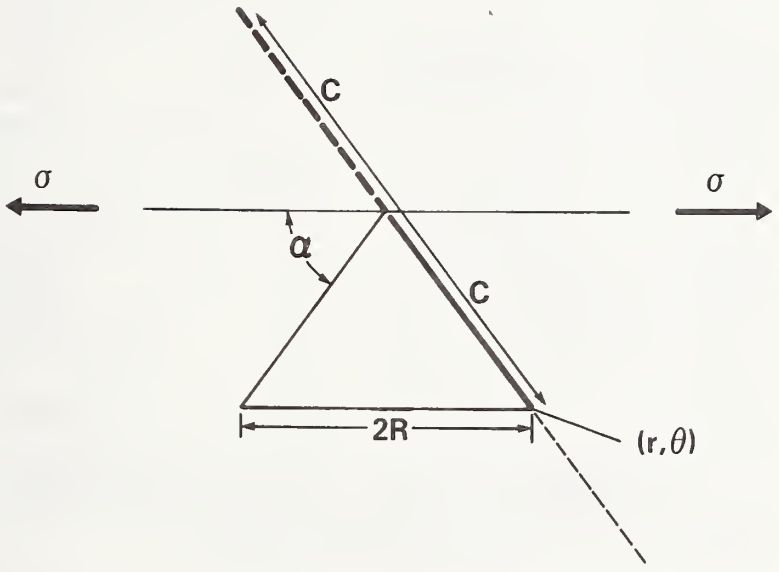

Al. Plane-crack representation of Hertzian cone configuration (side view). One seeks the crack increment at ($\underline{r}$, $\underline{\theta}$), with respect to origin at tip of representative crack, which optimizes energy release conditions.

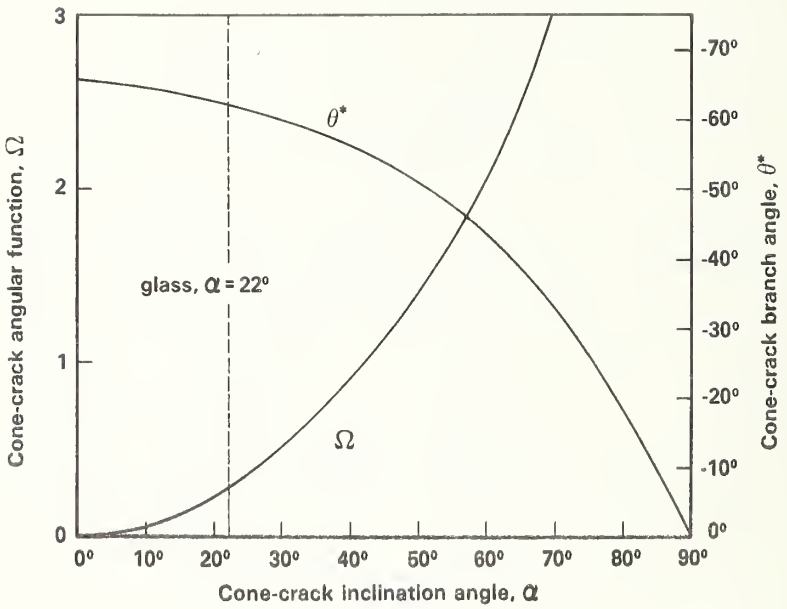

A2. Angular terms for cone-crack extension in tensile field.

DISTRIBUTION LIST

Organization

Office of Naval Research
Department of the Navy
Attn: Code 471
Arlington, Virginia 22217

Director
Office of Naval Research
Branch Office
495 Summer Street
Boston, Massachusetts 02210

Director
Office of Naval Research
New York Area Office
207 West 24th Street
New York, New York 10011

Director
Office of Naval Research
Branch Office
1030 East Green Street
Pasadena, California 91101

Commanding Officer
Naval Weapons Laboratory
Attn: Research Division
Dahlgren, Virginia 22448

Director
Naval Research Laboratory
Attn: Technical Information Officer
Code 2000
Washington, D. C. 20390

Director
Naval Research Laboratory
Attn: Technical Information Officer
Code 2020
Washington, D. C. 20390

Director
Naval Research Laboratory
Attn: Technical Information Officer
Code 6000
Washington, D. C. 20390

Organization

Director
Naval Research Laboratory
Attn: Technical Information Officer
Code 6100
Washington, D. C. 20390

Director
Naval Research Laboratory
Attn: Technical Information Officer
Code 6300
Washington, D. C. 20390

Director
Naval Research Laboratory
Attn: Technical Information Officer
Code 6400
Washington, D. C. 20390

Director
Naval Research Laboratory
Attn: Library
Code 2029 (ONRL)
Washington, D. C. 20390

Commander
Naval Air Systems Command
Department of the Navy
Attn: Code AIR 320A
Washington, D. C. 20360

Commander
Naval Air System Command
Department of the Navy
Attn: Code AIR 5203
Washington, D. C. 20360

Commander
Naval Ordnance Systems Command
Department of the Navy
Attn: Code ORD 033
Washington, D. C. 20360

Commanding Officer
Naval Air Development Center
Aeronautical Materials Div.
Johnsville
Attn: Code MAM
Warminster, Pa. 18974

Commanding Officer
Naval Ordnance Laboratory
Attn: Code 210
White Oak
Silver Spring, Maryland 20910

Commander
Naval Ship Systems Command
Department of the Navy
Attn: Code 0342
Washington, D. C. 20360

Commanding Officer
Naval Civil Engineering Laboratory
Attn: Code L70
Port Hueneme, California 93041

Commander
Naval Ship Engineering Center
Department of the Navy
Attn: Code 6101
Washington, D. C. 20360

Naval Ships R&D Laboratory
Annapolis Division
Attn: Code A800
Annapolis, Maryland 21402

Commanding Officer
Naval Ships R&D Center
Attn: Code 747
Washington, D. C. 20007

Commander Naval Weapons Center
Naval Weapons Center
Attn: Code 5560
China Lake, California 93555

Commander
Naval Underseas Warfare Center
Pasadena, California 92152

Scientific Advisor
Commandant of the Marine Corps
Attn: Code AX
Washington, D. C. 20380

Commanding Officer
Army Research Office, Durham
Box CM, Duke Station
Attn: Metallurgy & Ceramics Div.
Durham, North Carolina 27706

Office of Scientific Research
Department of the Air Force
Attn: Solid State Div. (SRPS)
Washington, D. C. 20333

Defense Documentation Center
Cameron Station
Alexandria, Virginia 22314

National Bureau of Standards
Attn: Metallurgy Division
Washington, D. C. 20234

National Bureau of Standards
Attn: Inorganic Materials Div.
Washington, D. C. 20234

Atomic Energy Commission
Attn: Metals & Materials Branch
Washington, D. C. 20545

Argonne National Laboratory
Metallurgy Division
P. O. Box 299
Lemont, Illinois 60439

Brookhaven National Laboratory
Technical Information Division
Attn: Research Library
Upton, Long Island, New York 11973

Library
Bldg. 50, Room 134
Lawrence Radiation Laboratory
Berkeley, California 94720

Los Alamos Scientific Laboratory
P. O. Box 1663
Attn: Report Librarian
Los Alamos, New Mexico 87544

Commanding Officer
Army Materials and Mechanics
Research Center
Attn: Res. Programs Office (AMXMR-P)
Watertown, Massachusetts 02172

Director
Metals & Ceramics Division
Oak Ridge National Laboratory
P. O. Box X
Oak Ridge, Tennessee 37830

Commanding Officer
Naval Underwater Systems Center
Newport, Rhode Island 02844

Aerospace Research Laboratories
Wright-Patterson AFB
Building 450
Dayton, Ohio 45433

Defense Metals Information Center
Battelle Memorial Institute
505 King Avenue
Columbus, Ohio 43201

Army Electronics Command
Evans Signal Laboratory
Solid State Devices Branch
c/o Senior Navy Liaison Officer
Fort Monmouth, New Jersey 07703

Commanding General
Department of the Army
Frankford Arsenal
Attn: ORDBA-1320, 64-4
Philadelphia, Pennsylvania 19137

Executive Director
Materials Advisory Board
National Academy of Sciences
2101 Constitution Avenue, N. W.
Washington, D. C. 20418

NASA Headquarters
Attn: Code RRM
Washington, D. C. 20546

Air Force Materials Lab
Wright-Patterson AFB
Attn: MAMC
Dayton, Ohio 45433

Air Force Materials Lab
Wright-Patterson AFB
Attn: MAAM
Dayton, Ohio 45433

Deep Submergence Systems Project
Attn: DSSP-00111
Washington, D. C. 20360

Advanced Research Projects Agency
Attn: Director, Materials Science
Washington, D. C. 20301

Department of the Interior
Bureau of Mines
Attn: Science & Engineering Advisor
Washington, D. C. 20240

Defense Ceramics Information Center
Battelle Memorial Institute
505 King Avenue
Columbus, Ohio 43201

National Aeronautics & Space Adm.
Lewis Research Center
Attn: Librarian
21000 Brookpark Rd.
Cleveland, Ohio 44135

Naval Missile Center
Materials Consultant
Code 3312-1
Point Mugu, California 93041

Commanding Officer
Naval Weapons Center Corona Labs.
Corona, California 91720

Commander
Naval Air Test Center
Weapons Systems Test Div. (Code 01A)
Patuxent River, Maryland 20670

Director
Ordnance Research Laboratory
P. O. Box 30
State College, Pennsylvania 16801

Director
Applied Physics Laboratory
1013 Northeast Fortieth St.
Seattle, Washington 98105

Materials Sciences Group
Code S130.1
271 Catalina Boulevard
Navy Electronics Laboratory
San Diego, California 92152

Dr. Waldo K. Lyon
Director, Arctic Submarine Laboratory
Code 90, Building 371
Naval Undersea R&D Center
San Diego, California 92132

Dr. R. Nathan Katz
Ceramics Division
U.S. Army Materials & Mechanics
Research Center
Watertown, Mass. 02172

SUPPLEMENTARY DISTRIBUTION LIST

Professor R. Roy
Materials Research Laboratory
Pennsylvania State University
University Park, Pennsylvania 16802

Professor D. H. Whitmore
Department of Metallurgy
Northwestern University
Evanston, Illinois 60201

Professor J. A. Pask
Department of Mineral Technology
University of California
Berkeley, California 94720

Professor D. Turnbull
Div. of Engineering and Applied Sci.
Harvard University
Pierce Hall
Cambridge, Massachusetts 02100

Dr. T. Vasilos
AVCO Corporation
Research and Advanced Development Div.
201 Lowell St.
Wilmington, Massachusetts 01887

Dr. H. A. Perry
Naval Ordnance Laboratory
Code 230
Silver Spring, Maryland 20910

Dr. Paul Smith
Crystals Branch, Code 6430
Naval Research Laboratory
Washington, D. C. 20390

Dr. A. R. C. Westwood
RIAS Division
Martin-Marietta Corporation
1450 South Rolling Road
Baltimore, Maryland 21227

Dr. W. Haller
Chief, Inorganic Glass Section
National Bureau of Standards
Washington, D. C. 20234

Dr. R. H. Doremus
General Electric Corporation
Metallurgy and Ceramics Lab.
Schenectady, New York 12301

Professor G. R. Miller
Department of Ceramic Engineering
University of Utah
Salt Lake City, Utah 84112

Dr. T. D. Chikalla
Fuels and Matls. Department
Battelle Northwest
P. O. Box 999
Richland, Washington 99352

Mr. I Berman
Army Materials and Mechanics
Research Center
Watertown, Massachusetts 02171

Dr. F. F. Lange
Westinghouse Electric Corporation
Research Laboratories
Pittsburgh, Pennsylvania 15235

Professor H. A. McKinstry
Pennsylvania State University
Materials Research Laboratory
University Park, Pa. 16802

Professor T. A. Litovitz
Physics Department
Catholic University of America
Washington, D. C. 20017

Dr. R. J. Stokes
Honeywell Corporate Research Center
10701 Lyndale Avenue South
Bloomington, Minnesota 55420

Dr. Harold Liebowitz
Dean of Engineering
George Washington Univeristy
Washington, D. C. 20006

Dr. H. Kirchner
Ceramic Finishing Company
P. O. Box 498
State College, Pennsylvania 16801

Professor A. H. Heuer
Case Western Reserve University
University Circle
Cleveland, Ohio 44106

Dr. D. E. Niesz
Battelle Memorial Institute
505 King Avenue
Columbus, Ohio 43201

Dr. F. A. Kroger
University of Southern California
University Park
Los Angeles, California 90007

Dr. Sheldon M. Wiederhorn
National Bureau of Standards
Inorganic Materials Division
Washington, D. C. 20234

Dr. C. O. Hulse
United Aircraft Research Labs
United Aircraft Corporation
East Hartford, Connecticut 06108

Professor M. H. Manghnani
University of Hawaii
Hawaii Institute of Geophysics
2525 Correa Road
Honolulu, Hawaii 96822

Dr. Stephen Malkin
Department of Mechanical Engineering
University of Texas
Austin, Texas 78712

Prof. H. E. Wilhelm
Department of Mechanical Engineering
Colorado State University
Fort Collins, Colorado 80521

Stanford University
Dept. of Materials Sciences
Stanford, California 94305

Dr. R. K. MacCrone
Department of Materials Engineering
Rensselaer Polytechnic Institute
Troy, New York 12181

Dr. D. C. Mattis
Belfer Graduate School of Science
Yeshiva University
New York, New York 10033

Professor R. B. Williamson
College of Engineering
University of California
Berkeley, California 94720

Professor R. W. Gould
Department of Metallurgical
and Materials Engineering
College of Engineering
University of Florida
Gainesville, Florida 32601

Professor V. S. Stubican
Department of Materials Science
Ceramic Science Section
Pennsylvania State University
University Park, Pennsylvania 16802

Dr. R. C. Anderson
General Electric Company
Miniature Lamp Department
Nela Park
Cleveland, Ohio 44112

Dr. Bert Zauderer
MHD Program, Advanced Studies
Room L-9513-VFSC
General Electric Company
P. O. Box 8555
Philadelphia, Pennsylvania 19101

Prof. C. F. Fisher, Jr.
Department of Mechanical and Aero-
Space Engineering
University of Tennessee
Knoxville, Tennessee 37916

USCOMM-NBS-DC

NBS-114A (REV. 7-73)

U.S. DEPT. OF COMM. BIBLIOGRAPHIC DATA SHEET	1. PUBLICATION OR REPORT NO. NBSIR 75-664	2. Gov't Accession No.	3. Recipient's Accession No.

4. TITLE AND SUBTITLE

Strength Degradation of Brittle Surfaces: Blunt Indenters

5. Publication Date February 1975

6. Performing Organization Code

7. AUTHOR(S)

B. R. Lawn; S. M. Wiederhorn; H. H. Johnson

8. Performing Organ. Report No.

9. PERFORMING ORGANIZATION NAME AND ADDRESS

NATIONAL BUREAU OF STANDARDS
DEPARTMENT OF COMMERCE
WASHINGTON, D.C. 20234

10. Project/Task/Work Unit No. 3130453

11. Contract/Grant No.

12. Sponsoring Organization Name and Complete Address (Street, City, State, ZIP)

Department of the Navy
Office of Naval Research
Arlington, Virginia 22217

13. Type of Report & Period Covered Interim 7/74 - 6/30/75

14. Sponsoring Agency Code ONR

15. SUPPLEMENTARY NOTES

16. ABSTRACT *(A 200-word or less factual summary of most significant information. If document includes a significant bibliography or literature survey, mention it here.)*

Indentation fracture mechanics is used to develop a theoretical basis for pre-determining the strength properties of brittle surfaces in prospective contact situations. Indenters are classified as "blunt" or "sharp," of which only the first is considered in the present work. The classical Hertzian cone crack conveniently models the fracture damage incurred by the surface in this class of indentation event. Significant degradation is predicted to occur at a critical contact load; however, with increasing load beyond this critical level the degradation rate becomes relatively slight. Bend tests on abraded glass slabs confirm the essential features of the theoretical predictions. The role of controlling variables in the degradation process, notably starting flaw size and indenter radius, is systematically investigated. An indication is also given as to optimisation of material parameters. The analysis leads to some novel suggestions concerning surface preparation procedures that might be followed in order to minimize strength losses.

17. KEY WORDS *(six to twelve entries; alphabetical order; capitalize only the first letter of the first key word unless a proper name; separated by semicolons)*

Brittle solids; ceramic surfaces; cracks; degradation; fracture; Hertzian; indentation; strength

18. AVAILABILITY [XX] Unlimited

[ ] For Official Distribution. Do Not Release to NTIS

[ ] Order From Sup. of Doc., U.S. Government Printing Office Washington, D.C. 20402, SD Cat. No. C13

[ ] Order From National Technical Information Service (NTIS) Springfield, Virginia 22151

19. SECURITY CLASS (THIS REPORT) UNCLASSIFIED

21. NO. OF PAGES 31

20. SECURITY CLASS (THIS PAGE) UNCLASSIFIED

22. Price